

Simulating the transportation and dispersal of volcanic ash cloud with initial condition created by 3D plume model

Zhixuan Cao^{1,2} Bursik Marcus³ Qingyuan Yang^{4,5} Abani Patra^{1,6}

¹ MAE Department, SUNY Buffalo, Buffalo, NY, USA

² Fluids Business Unit, ANSYS Inc, Lebanon, NH, USA

³ Geology Department, SUNY Buffalo, Buffalo, NY, USA

⁴ Earth Observatory of Singapore, Singapore, Singapore

⁵ The Asian School of the Environment, Nanyang Technological University, Singapore, Singapore

⁶ Computer Science, School of Engineering, Tufts, Boston, MA, USA

Correspondence*:

Corresponding Author

email@uni.edu

2 ABSTRACT

3 VATDs (volcanic ash transportation and dispersion) model atmospheric transport of ash starting
4 from a source originating at the volcano represented by concentrations of ash with height.
5 Most VATD models use a source of some prescribed shape calibrated against an empirical
6 expression for the height-mass eruption rate (MER) relation. The actual vertical ash distributions
7 in volcanic plume usually vary from case to case and have complex dependencies on eruption
8 source parameters and atmospheric conditions. We present here for the first time the use of
9 3D (three-dimensional) plume models to represent ash cloud sources without any assumption
10 regarding plume geometry. By eliminating assumed behavior associated with the semiempirical
11 plume geometry, the predictive skill of VATD simulations are greatly improved. To date no VATD
12 simulation adopts the initial condition created from first principles based 3D plume simulation. We
13 use our recently developed volcanic plume model based on a 3D Lagrangian method [Cao et al,
14 Geophysical Model Dev., 2018] and couple the output to a standard Lagrangian VATD model and
15 apply to historical eruptions to illustrate the effectiveness of this approach. The importance of
16 the source model is shown in sensitivity analyses which prove that volcanic ash transportation
17 simulation is much more sensitive to the source geometry than all other input parameters. Further
18 investigation also reveals that initial particle distribution in vertical direction has more impact
19 on transportation of ash clouds than horizontal distribution. Comparison also indicates that ash
20 particles are concentrated along the intrusion height of umbrella cloud that is much lower than
21 the plume top, which is just momentum overshoot.

22 **Keywords:** VATD, volcano, ash cloud, 3D plume model, initial condition, numerical simulation, SPH, Pinatubo

1 INTRODUCTION

23 The fine-grain fraction of tephra (volcanic ash) can be widely dispersed, and can lead to a degradation of
24 air quality and pose threats to aviation (Tupper et al., 2007). Identification of volcanic ash helps schedule

flights to avoid areas where ash is present. Numerical estimation of ash distribution using known and forecast wind fields is necessary if we are to accurately predict ash cloud evolution. Numerous VATD (volcanic ash transportation and dispersion) models have been developed by both civil and military aviation or meteorological agencies to provide forecasts of ash cloud motion (Witham et al., 2007). New techniques have been integrated with VATDs to satisfy increasing demands for more outputs, model accuracy and forecast reliability. This contribution explores a method for creating initial conditions for VATD simulations, which promises to improve prediction capability and accuracy.

Fero et al. (2009) and Stohl et al. (2011) showed that initial source conditions have significant effects on simulation of volcanic ash transportation. Traditional VATD simulation requires key global descriptors of the volcanic plumes, especially plume height, grain size, eruption duration and mass loading, or alternatively, a mass eruption rate (MER). No matter how these global descriptors are obtained, they are used to furnish the initial conditions for VATDs in the form of a line-source term of a spatio-temporal distribution of particle mass. It is a common practice to pick values for these global descriptors using an empirical expression for the height-MER relation. The empirical expression is written as a function of several parameters, including the key global descriptors. The values for the descriptors can also be found by parameter calibration (e.g. Fero et al., 2008, 2009; Stohl et al., 2011; Zidikheri et al., 2017). 1D plume models serve as an alternative option to provide values. For example, Bursik et al. (2012) used the 1D model puffin (Bursik, 2001) to generate estimates of mass eruption rate and grain size. In some cases, an extra step is adopted to spread ash particles from the line source horizontally, resulting in an initial ash cloud in 3D space. The horizontal spreading depends on an empirical expression. For example, the VATD model Puff spreads particles from the line source uniformly in the horizontal direction within a given radius using an empirical expression in puffin. Considering the complexities of volcanic eruptions, the actual ash distribution in initial ash clouds should vary from case to case and with time, making it difficult to find one general expression that is suitable for all cases. It is useful therefore to investigate alternative ways for creating initial ash clouds without assumptions regarding plume geometry or numerical inversion. This provides the major motivation of this paper.

VATD models can be categorized into Lagrangian particle tracking and Eulerian advection-diffusion types. Among several available particle tracking models (e.g. Walko et al., 1995; Searcy et al., 1998; D'amours, 1998; Draxler and Hess, 1998) and advection-diffusion models (e.g. Bonadonna and Houghton, 2005; Folch et al., 2009; Schwaiger et al., 2012), we adopt a particle tracking model, Puff (Tanaka, 1991; Searcy et al., 1998), as the primary VATD model. Puff can take 3D ash clouds as initial conditions, which makes it technically easier to couple with 3D plume models. Puff initializes a discrete number of tracers that represent a sample of the eruption cloud, and calculates transport, turbulent dispersion, and fallout for each representative tracer. A cylinder emanating vertically from the volcano summit to a specified maximum height is the standard approach to provide a simple model of the geometry of a typical ash column. Puff minimally requires horizontal wind field data. The “restart feature” of Puff makes it technically feasible to accommodate the hand-off between a plume simulation and the Puff simulation in terms of time and length scales.

We also use another one of the most widely used models for atmospheric trajectory and dispersion calculations, the Hybrid Single-Particle Lagrangian Integrated Trajectory model (HYSPLIT) (Stein et al., 2015; Rolph et al., 2017), developed by NOAA's Air Resources Laboratory. HYSPLIT is able to simulate simple back trajectories to very sophisticated computations of transport, mixing, chemical transformation, and deposition of pollutants and hazardous materials. It is used in this study to better understand simulation results by Puff.

69 Besides parameter calibration, 1D (one dimensional) plume models have been used to obtain global descri-
70 ptors of volcanic plumes. 1D plume models (e.g. Woods, 1988; Bursik, 2001; Mastin, 2007; de'Michieli
71 Vitturi et al., 2015; Folch et al., 2016; Pouget et al., 2016) solve the equations of motion in 1D using
72 simplifying assumptions, and hence depend on estimation of certain parameters, especially those related to
73 the entrainment of air, which is evaluated based on two coefficients: a coefficient due to turbulence in the
74 rising buoyant jet, and one due to the crosswind field. Different 1D models adopt different entrainment
75 coefficients based on a specific formulation or calibration against well-documented case studies. The
76 feedback from plume to atmosphere is usually ignored in 1D models. While these 1D models generated
77 well-matched results with 3D models for plumes that are dominated by wind (often called weak plumes)
78 much greater variability is observed for strong plume scenarios (Costa et al., 2016). On the other hand, 3D
79 numerical models for volcanic plumes based on first principles and having few parametrized coefficients
80 (Oberhuber et al., 1998; Neri et al., 2003; Suzuki et al., 2005; Cerminara et al., 2016a; Cao et al., 2018)
81 naturally create a 3D ash cloud, which could serve directly as an initial state of the volcanic material for
82 VATDs. However, there is no VATD simulation using such 3D ash clouds as initial conditions. In this paper,
83 we will carry out VATD simulations using an initial state for the ash cloud based on 3D plume simulations,
84 generated with Plume-SPH (Cao et al., 2018, 2017). The implementation techniques described in this paper
85 can be applied for any combination of VATD model and 3D plume model even though our investigation is
86 based on a specific VATD model and plume model.

87 The 1991 eruption of Pinatubo volcano is used as a case study. Pinatubo erupted between June 12 and 16,
88 1991, after weeks of precursory activity. The climactic phase started on June 15 at 0441 UTC and ended
89 around 1341 UTC (Holasek et al., 1996a). The climactic phase generated voluminous pyroclastic flows,
90 and sent Plinian and co-ignimbrite ash and gas columns to great altitudes (Scott et al., 1996). The evolution
91 of the Pinatubo ash and SO_2 clouds was tracked using visible (Holasek et al., 1996a), ultraviolet (Total
92 Ozone Mapping Spectrometer; TOMS) (Guo et al., 2004a) and infrared sensors, including the Advanced
93 Very High-Resolution Radiometer (AVHRR) (Guo et al., 2004b). There is also sufficient observational data
94 to estimate the eruption conditions for the climactic phase of the eruption (Suzuki and Koyaguchi, 2009).
95 The availability of calibrated eruption conditions and extensive observational data regarding ash clouds
96 transport make the Pinatubo eruption an ideal case study.

2 MATERIALS AND METHODS

2.1 Creation of Initial Ash Cloud

98 The steps to create an initial ash cloud based on the raw output of Plume-SPH are shown in Fig. 1.
99 The method proposed consists in generating the initial ash cloud directly from Plume-SPH, foregoing
100 assumptions and estimates or inverse modeling regarding ash injection height and timing thereof. We use
101 Plume-SPH as an example, noting that for other 3D plume models, the steps would be similar. Plume-SPH
102 is a two-phase model based on the Lagrangian smoothed-particle hydrodynamics (SPH) method, in which
103 the computational domain is discretized by SPH particles. The current version, Plume-SPH 1.0 (Cao et al.,
104 2018), uses two types of SPH particles: 1) particles of phase 1 to represent ambient air, and 2) particles of
105 phase 2 to represent erupted material. The initial ash cloud is created from SPH particles of phase 2.

106 After reaching the maximum rise height and starting to spread horizontally, particles of phase 2 form an
107 initial umbrella cloud (Fig. 2). The 3D plume simulation is considered complete once the umbrella cloud
108 begins to form. Parcels that will be transported by the ambient wind are those above the “corner” region,
109 where mean plume motion is horizontal rather than vertical.

Considering that SPH particles are only discretization points, each is assigned a grain size according to a given total grain size distribution (TGSD) (Paladio-Melosantos et al., 1996), and a concentration according to the mass and volumetric eruption rate. The Plume-SPH discretization points are thus switched to Puff Lagrangian tracer particles having grain sizes and concentrations. The coordinates of these tracer particles, which are initially in the local Cartesian coordinate system of Plume-SPH, are converted into Puff's global coordinate system, which is given in terms of (*longitude, latitude, height*). Puff takes the initial ash cloud, consisting of the collection of Lagrangian tracer particles with grain size and concentration, and propagates from time t to time $t + \Delta t$ via an advection/diffusion equation (Searcy et al., 1998).

$$\mathbf{R}_i(t + \Delta t) = \mathbf{R}_i(t) + \mathbf{W}(t)\Delta t + \mathbf{Z}(t)\Delta t + \mathbf{S}_i(t)\Delta t \quad (1)$$

Here, $\mathbf{R}_i(t)$ is the position vector of the i^{th} Lagrangian tracer particle at time t , \mathbf{W} accounts for wind advection, \mathbf{Z} accounts for turbulent dispersion and \mathbf{S} is the terminal gravitational fallout velocity, which depends on tracer's size.

To summarize, there are four steps to create an initial ash cloud from the raw output of Plume-SPH:

1. filter by SPH particle type to select SPH particles that represent erupted material (phase 2)
2. filter by a mean velocity threshold to select the upper part (above the “corner” region) dominated by horizontal transport
3. switch SPH discretization points to Lagrangian tracer particles, by assigning grain size to each particle
4. convert coordinates of the SPH Lagrangian tracers into the VATDs' geographic coordinate system

The features of the volcanic plume and resulting initial ash cloud used in the case study are shown in Fig. 2. It is important to point out that since both Plume-SPH and Puff are based on the Lagrangian method, there is no extra step of conversion between an Eulerian grid and Lagrangian particles.

Table 1 compares three different methods for creating initial conditions for VATD simulation: 1) creating initial condition based on parameter calibration without any plume model (method 1), 2) creating initial condition based on output of 1D plume model (method 2), 3) extracting initial ash cloud from 3D plume simulation (method 3). The first method determines all global descriptors of volcanic plumes based on calibration. Then create an initial line source or ash cloud according to semiempirical plume shape expression. Both other two methods depend on plume models. However 3D plume models can generate initial ash clouds in 3D space while 1D plume models only obtain global descriptors of plume so still need semiempirical expression to create 3D initial ash clouds. In addition, the number of Lagrangian tracers is a free parameter when using semiempirical plume shape expressions while it purely depends on simulation when creating initial conditions from 3D plume simulation results.

2.2 Puff Restart

The plume and ash transport models are run at different time scales and length scales. The spatial and temporal resolutions of the plume simulations are much finer than those of the ash transport model. It takes tens of minutes (600s in this case) for the Pinatubo plume to reach a steady height. However the eruption persisted for a few hours (9 hours for the climactic phase of Pinatubo eruption), and it may be necessary to track ash transport for days following an eruption. At present, it is too expensive computationally to do 3D plume simulations of several hours in real time. In order to handle the difference in time scale, we mimic a continuing eruption with intermittent pulsed releasing of ash particles. Particularly, we restart Puff at an interval of 600s, i.e., the physical time of the plume simulation to reach steady height. At every Puff restart, we integrate the output of the last Puff simulation and Plume-SPH into a new ash cloud. This

new ash cloud serves as a new initial condition with which to restart a Puff simulation. The interval of the pulsed releases is the simulation time of Plume-SPH, i.e., 600s in our case study. A sketch demonstrating the overall restart process is shown in Fig. (3). The total number of Lagrangian tracer particles used in Puff thus equals the summed number of particles in all releases. So the total number of tracer particles is no longer a user-selected parameter. Fero et al. (2008) proposed using more realistic time-dependent plume heights. We do not adopt that strategy here for simplicity, although the idea would be straightforward in execution, given time-dependent eruption conditions.

2.3 Sensitivity Analysis of Other Parameters

Besides the positions of particles in the initial ash cloud, other parameters for Puff simulations are: horizontal diffusivity, vertical diffusivity, mean grain size, grain size standard deviation and total number of tracers. We present in this subsection systematic sensitivity studies on these parameters. We also investigate the influence of eruption duration. The sensitivity analyses will serve as the basis for identifying possible sources of disparities between simulation and observation.

The sensitivity analyses illustrate that adjustment of other parameters produces negligible visual differences in VATD simulation results. Using different vertical diffusivities in range of $[100, 100000]m^2 s^{-1}$ and different horizontal diffusivities in range of $[1, 20]m^2 s^{-1}$ produces visually negligible differences. The simulation eruption duration should depend on the total observed duration or the duration of the climactic phase. We conducted several simulations with eruption duration varying in range of $[5, 11]hours$ with slightly different starting time of climactic phase. Table 2 lists all these simulations. However, only tiny visible differences are observed among the simulated ash transportation. The mean of grain size also has visually ignorable effects on long-term ash transportation according to our sensitivity tests varying the log mean (base 10) grain radius in a range of $[-7.3, -3.5]m$. The standard deviation, when varying in range of $[0.1, 10]$, generates an ignorable difference on long-term ash transportation as well. Similar conclusion on parameter sensitivity is reported by Fero et al. (e.g. 2008); Daniele et al. (e.g. 2009). Among these parameters, the eruption duration and beginning time shows, even though tiny, the most obvious influence on simulated ash distribution. In order to show such differences in an intuitive way, Fig. ?? shows simulated ash distribution corresponding to 4.9 hours duration, 9 hours duration and 11 hours duration respectively. After 72 hours, relative to the simulation starting time, these three cases generate generally similar results, with high concentration ash covering almost the same region. The difference of lower concentration distribution is relatively more obvious. Ash cloud covers the broadest area when the eruption duration is 11.1 hours. To summarize, all these parameters have either tiny or ignorable effects on long-term ash distribution simulation.

The new methodology for generating initial ash clouds introduces another new parameter: elevation threshold. We also carry out sensitivity analysis on this parameter by varying the elevation threshold from 1500m (the height of the vent) to 25000m. The simulated ash distributions show obviously visible differences. Such influence is especially obvious when the elevation threshold is either very large or very small. However, varying the elevation threshold in the range of $[12000, 18000]m$ generates relatively small differences in ash transportation simulation results. Subfigure d) and e) in Figure 4 compares the simulated ash distribution corresponding to elevation thresholds of 1500m and 15000m. Compared with ash distribution for threshold of 15000m, an extra long tail appears when using elevation threshold of 1500m. Adopting smaller elevation thresholds essentially adds more tracers at lower elevation. As the wind at different elevations are different, these tracers at lower elevation would transpose to different directions. The HYSPLIT (Stein et al., 2015; Rolph et al., 2017) forward trajectories tracking, which starting at June

194 15 1624 UTC, indicates that the wind between evaluation 10000 m to 15000 m blows from north-east to
195 south-west while wind of higher evaluation blows from east to west (see Fig. 5).

196 The sensitivity analyses demonstrate that the initial condition for VATD simulation has the most significant
197 effect on simulated ash distribution while all other input parameters have either tiny or ignorable influence.
198 The initial ash cloud generated based on semiempirical expression, which is a function of several parameters,
199 might be significantly disparate from a realistic ash cloud. Such initial conditions might greatly compromise
200 the accuracy of VATDs simulation.

201 In this paper, we do not carry out any investigation with respect to wind field even though it is another
202 dominant factor in VATD simulation. In the case study, we use global NOAA/OAR/ESRL6 – h , 2.0°
203 reanalysis wind fields data (Whitaker et al., 2004; Compo et al., 2006, 2011).

3 RESULTS

204 Transportation of volcanic ash resulting from the Pinatubo eruption on June 15th 1991 is simulated using
205 two different initial conditions. The first type of initial condition is created in a traditional way according
206 to key global descriptors and semiempirical plume shape expression. The second type of initial condition
207 is created by the new method proposed in this paper. Simulated ash transportation results are compared
208 against observations.

209 To create initial conditions using the new method described in this paper, the plume rise is simulated first
210 by Plume-SPH. The eruption parameters, material properties and atmosphere for the strong plume no wind
211 case in a comparison study on eruptive column models (Costa et al., 2016) are adopted. Eruption conditions
212 and material properties are listed in Table 3. Note that the density of erupted material at the vent and radius
213 of the vent can be computed from the given parameters. The eruption pressure is assumed to be the same as
214 the pressure of ambient at the vent and hence is not given in the table. The vertical profiles of atmospheric
215 properties were obtained based on the reanalysis data from ECMWF (European Centre for Medium-Range
216 Weather Forecasts) for the period corresponding to the climactic phase of the Pinatubo eruption. The initial
217 ash cloud is obtained by processing the raw output of Plume-SPH following steps described in Sec. 2.

218 Another set of initial conditions is created based on observed top height (40km) and several other
219 parameters assigned semiempirically (Bursik et al., 2012). These parameters, namely, the global descriptors
220 of volcanic plume, are used as parameters of semiempirical expression to get ash clouds in 3D space. See
221 details in Table 4. Except for initial conditions, the simulation parameters that control VATD simulation are
222 the same for both simulations. As has been shown in the sensitivity analyses section, these parameters have
223 less influence on simulation results than initial condition.

224 The simulation results using different initial conditions are compared with TOMS images and AVHRR
225 BTD ash cloud map in Fig. 6.

226 The differences between simulated ash transportation by “Semiempirical initial cloud +Puff” and “Plume-
227 SPH+Puff” are obvious. The simulated ash concentration based on initial condition created from Plume-
228 SPH is much closer to observation than that based on semiempirical plume shape expression. Around 23
229 hours and 31 hours after the beginning of the climactic phase, “Plume-SPH + Puff” simulation generates ash
230 images that are generally close to observational images, especially the location where high concentration
231 ash presents. However, these ash at near west to Pinatubo mountain observed in satellite images does not
232 show up in “Plume-SPH + Puff” simulation results. This disparity is very possible due to the fact that the
233 Mountain Pinatubo continued erupting after the climactic phase while our simulation only simulates the
234 climactic phase. The ash released after the climactic phase is not accounted for in our simulation results. The

235 “Semiempirical initial cloud + Puff” simulation, however, forecasts an ash distribution faster and narrower
 236 than observation. The location, where the high concentration ash presents, is located to the far northwest of
 237 observed ash. Around 55 hours after the beginning of the climactic phase, the disparity between observation
 238 and simulation becomes more obvious. Ash distribution of “Semiempirical initial cloud + Puff” simulation
 239 locates far west to the observed ash. The high concentration area of “Plume-SPH + Puff” simulation, even
 240 though closer to observation than that of “Semiempirical initial cloud +Puff”, is still faster than observation.

241 Except for the initial condition, both simulations adopt the same parameters and wind field data. That
 242 is to say, the only difference between these two simulations is the initial condition. Recall that the initial
 243 condition has the most significant influence on ash transportation simulation. It is therefore very likely
 244 that the big difference between simulation results by “Plume-SPH+Puff” and “Semiempirical initial cloud
 245 +Puff” may be attributed to the initial condition and thereby be credited with its added skill.

4 DISCUSSION

4.1 Discussion Regarding Maximum Height (H_{max})

247 In this section, we mainly discuss the vertical distribution of ash particles in the initial ash cloud. The
 248 majority of volcanic ash particles usually present a lower elevation than maximum height. For instance,
 249 Holasek et al. (1996a,b) reported the maximum Pinatubo plume height as high as around 39km while the
 250 cloud heights were estimated at 20 ~ 25km, Self et al. (1996) report the maximum plume height could
 251 be > 35km and the plume heights are 23 ~ 28km after 15 ~ 16 hours. The neutral buoyant regions of
 252 the Pinatubo aerosol estimated by different measurements are: 17 ~ 26km (lidar) by DeFoor et al. (1992),
 253 20 ~ 23km (balloon) by Deshler et al. (1992), 17 ~ 28km (lidar) by Jäger (1992), and 17 ~ 25km (lidar)
 254 by Avdyushin et al. (1993). Based on comparison between simulated clouds with early infrared satellite
 255 images of Pinatubo, Fero et al. (2008) reported that the majority of ash was transported between 16km
 256 and 18km. This is physically understandable as particles are concentrated along the intrusion height of
 257 the umbrella cloud, not near the top because the plume top is due to momentum overshoot. However, the
 258 empirical expressions for the height-MER relation, which are commonly adopted to create initial conditions
 259 for VATD simulation, tend to place the majority of ash particles closer to top if use observed maximum
 260 height in the empirical expressions.

261 Here we check two commonly used plume shapes, the Poisson and Suzuki. For Poisson plume shape, the
 262 vertical height of ash particles are determined according to Eq. (2).

$$H = H_{max} - 0.5H_{width} * P + H_{width}R \quad (2)$$

263 where P is an integral value drawn from a Poisson distribution of unit mean, R is a uniformly distributed
 264 random number between 0 and 1, H_{max} is the maximum plume height, H_{width} represents an approximate
 265 vertical range over which the ash will be distributed. For Suzuki plume shape (Suzuki et al., 1983), volcano
 266 ash mass vertical distribution is assumed to follow the Suzuki equation (Eq. (3)).

$$Q(z) = Q_m * \frac{k^2(1 - z/H_{max})\exp(k(z/H_{max} - 1))}{H_{max}[1 - (1 + k)\exp(-k)]} \quad (3)$$

267 Where Q_m is the total mass of erupted material, k is shape factor, which is an adjustable constant that
 268 controls ash distribution with height. A low value of k gives a roughly uniform distribution of mass with
 269 elevation, while high values of k concentrate mass near the plume top.

270 Particle distribution (in terms of mass percentage or particle number percentage) in vertical direction
271 in the initial ash cloud are shown in Fig. 7. In that figure, the vertical particle distribution based on
272 Plume-SPH output is compared with vertical particle distribution created based on semiempirical shape
273 expressions. Both Poisson and Suzuki distribution in Fig. 7 take $H_{max} = 40000m$, which is close to
274 reported observation of maximum height. When adopting Poisson plume shape, the majority of the particles
275 are between $30km \sim 40km$. Obviously, Poisson distributes majority ash at a much higher elevation than
276 observations (e.g. Fero et al., 2008). As for Suzuki, the majority of ash particles also distribute in a range
277 that is significantly higher than $25km$. As for initial ash clouds based on Plume-SPH simulation, the major
278 population of ash particles distribute between $17km \sim 28km$, which match well with observations. The
279 maximum height is also consistent with observation. To summarize, using semiempirical plume shape
280 expression generates an unrealistic initial ash cloud even if we use observed plume maximum height.

281 For Poisson and Suzuki plume shape, vertical distribution of ash particles can't be lower down without
282 changing the maximum height. To distribute a major population of ash particles at lower elevation, the
283 maximum height has to be reduced to a value smaller than observed maximum height. Adjusting parameters
284 such as maximum height in the empirical expression is actually the traditional source term calibration
285 method. A set of initial ash clouds using different maximum heights based on Poisson plume shape is
286 shown in Fig. 8). The maximum heights adopted in plume shape expressions are, by no means, obtained
287 from any plume model or observation. Except for maximum height, all other parameters for creating an
288 initial ash cloud are the same as these in Table 4. The range, between which major populations of ash
289 particles locate, is lower when using smaller maximum heights. These ash clouds created by Poisson
290 distribution with different maximum heights are then used as initial conditions in Puff simulation, whose
291 results are shown in Fig. 11.

292 Figure 11 shows that the maximum height has significant influence on ash transportation simulation.
293 When the maximum height is $10000m$ the high concentration area is lag behind observation. While the
294 designated maximum height is $35000m$, the high concentration area is a little bit faster and much narrower
295 than observation. When using a maximum height of $41343.9m$, the high concentration area is faster and
296 narrower than both observation and "Pume-SPH+Puff" simulation results (see Fig. 6). The simulated
297 high concentration area is closest to "Pume-SPH+Puff" simulation results when assigning a maximum
298 height of $30000m$. The front of volcano ash, with lower concentration is faster than observation located far
299 west to high concentration areas. A lower concentration tailing area also appears in the simulation results
300 while there is no such tail in the observed image. Puff simulation result based on calibrated maximum
301 height of $30000m$ shows similar footprint to, even though smaller in terms of covered area than, those of
302 "Pume-SPH+Puff" simulation. However, the initial ash cloud created by Poisson distribution with maximum
303 height around $20000m$ generates best match ash distribution with observation. That is to say, a maximum
304 height lower than real maximum height is required by Poisson plume shape to distribute ash particles at the
305 same elevation as real ash distribution. This is physically understandable as maximum plume heights are
306 reached due to overshoot. Our hypothesis regarding the sources of disparity between "Semiempirical initial
307 cloud +Puff" simulation and observation is confirmed. Since the initial condition has such a dominant
308 effect on VATD simulation, it is critical for the forecast capability of VATD simulation to explore the more
309 accurate and adaptive ways for establishing the initial conditions, especially the method that does not rely
310 on "post event" parameter calibration.

311 4.2 Discussion Regarding Vertical Spread (H_{width})

312 In the previous section, the maximum height is adjusted to change vertical ash distribution along the
313 source line. This section investigates another parameter in semi empirical Poisson expression. We vary the

314 “vertical spread” (H_{width}) in range $3km/10km$. A set of initial ash clouds created according to different
 315 “vertical spread” is shown in Fig. 8. Except for “vertical spread”, all other parameters for creating an initial
 316 ash cloud are the same as these in Table 4. Width of the range within which major populations of ash
 317 particles locate become narrower when a smaller value for vertical spread is used. But changing H_{width}
 318 has no obvious effect on the height at which the majority of ash particles distribute. These ash clouds based
 319 on different vertical spread are then used as initial conditions in Puff simulation, whose results are shown
 320 in Fig. 11.

321 Adjusting of the vertical spread can change particle distribution in vertical direction and not surprisingly
 322 affect VATD simulation results. Unluckily, none of these VATD simulations based on initial ash cloud with
 323 vertical spread equals to $3km$, $5km$, and $10km$ get better results than VATD simulation based on initial
 324 condition created by a 3D plume simulation using Plume-SPH (see Fig. 11).

325 The calibrations carried out here are definitely not exhaustive. One might do more comprehensive
 326 calibration throughout the multi-dimensional parameter space (for Poisson distribution, the parameter space
 327 is two dimensional) and get better matched ash transportation results. With more complicated plume shape
 328 expression, one could have more control over plume shape and might be able to get an initial condition that
 329 is much closer to the actual initial ash cloud, hence obtaining more accurate ash transportation prediction.
 330 But more complicated plume shape expression usually leads to higher dimensional parameter space which
 331 requires more effort to do calibration. Even though, the degree of freedom to adjust plume shape is still
 332 limited. The new method for creating initial conditions based on 3D plume simulation is more adaptive to
 333 various cases and obviates semi empirical expressions regarding plume shape.

334 4.3 Horizontal Ash Distribution

335 The differences between assumed plume particle distribution and actual (or simulated by 3D plume)
 336 model are not only in vertical direction. Dependence on horizontal particle distribution of the initial ash
 337 cloud on ash transportation is investigated in this section. Puff uses a uniformly distributed random process
 338 to determine the ash particle location in a circle centered on the volcano site. The maximum radius (at
 339 top) is given as “horizontal spread” in Table 4. The horizontal displacement from a vertical line above the
 340 volcano is a random value within a circle of radius, which equals to “horizontal spread” multiplied by the
 341 ratio of the particle height H to maximum H_{max} . So the net shape of the plume is an inverted cone where
 342 particles are located directly over the volcano at the lowest level and extend out further horizontally with
 343 increasing plume height. As for output of Plume-SPH, an effective radius is determined according to a given
 344 threshold of ash concentration following Cerminara et al. (2016b). A time averaging and spatial integration
 345 of the dynamic 3D flow fields are conducted to get rid of significant fluctuations in time and space. Fig. 9
 346 compares radius of initial ash clouds created by 3D plume simulation and assumed plume shape expression
 347 adopted in Puff. Obviously, It is impossible for the simple assumed plume shapes to capture the complex
 348 and more realistic shapes developed by 3D plume simulation of Plume-SPH. Additional parameterization
 349 may generate more reasonable shapes but none are likely to have the fidelity of the 3D simulation.

350 Comparison between cross-sectional views of the initial ash clouds is shown in Fig. 10. The cross-
 351 sectional view of assumed plume shape (last figure in Fig. 10) is similar to a cross-sectional view of
 352 simulated 3D plumes in general sense. However, for simulated 3D plume, the ash particle distribution on
 353 cross section varies along with height. It is hard for semiempirical expressions to have such a distribution.
 354 In Puff, particle distribution on cross sections is assumed to be the same.

355 Assigning different values to “horizontal spread” has an ignorable effect on VATD simulation results.
 356 We use numbers between $50km$ to $1600km$ as “horizontal spread” to create initial ash clouds for VATD,

357 all of them generate very similar results. Figure 11 shows two different simulation results based on initial
358 ash clouds with “horizontal spread” equals to 50km and 600km respectively. No visible differences are
359 apparent between them. This implies that horizontal distribution has less significant influence on VATD
360 simulation results than vertical distribution.

361 4.4 Summary

362 This paper presented, for the first time, VATD simulations using initial source conditions created by a 3D
363 plume model. Traditional VATD simulations use initial conditions created according to a semiempirical
364 plume shape expression. A case study of the 1991 Pinatubo eruption demonstrates that a 3D plume model
365 can create more realistic initial ash cloud and ash parcel positions, and therefore improve the accuracy of
366 ash transport forecasts. Informal sensitivity analyses suggest that initial conditions, as expressed in the
367 disposition of initial ash parcel positions in the vertical, have a more significant effect on a volcanic ash
368 transport forecast than most other parameters. Comparison of initial ash parcel distributions among the
369 3D plume model, semiempirical expressions, and observations suggests that a major subpopulation of ash
370 parcels should be placed at a much lower elevation than maximum height to obtain a better VATD forecast.
371 For the Pinatubo case study, “well-matched” simulation results are observed when using a maximum height
372 of around 30km, which is much lower than the observed maximum height of 40km. Comparing the effects
373 of the maximum height, vertical spread and horizontal spread shows that ash particle distribution in the
374 vertical direction has the strongest effect on VATD simulation.

375 To summarize, we have presented a novel method for creating *a priori* initial source conditions for
376 VATD simulations. We have shown that it might be possible to obtain initial positions of ash parcels
377 with deterministic forward modeling of the volcanic plume, obviating the need to attempt to obtain initial
378 positions or a history of release heights via inversion (Stohl et al., 2011). Although the method now
379 suffers from the high computational cost associated with 3D forward modeling, it not only helps overcome
380 shortcomings of existing methods used to generate *a priori* input parameters, but also overcomes the need
381 to do the thousands of runs associated with inverse modeling. In addition, computational cost will continue
382 to diminish as computing speed increases. As they are forward numerical models based on first principles,
383 3D plume models need little if any parameterization, and user intervention should not be required to
384 improve forecast power; no assumption about the initial position of ash parcels is needed. Generation of the
385 initial cloud of ash parcels directly by 3D simulation is potentially adaptable to a variety of volcanic and
386 atmospheric scenarios. In contrast, semiempirical expressions used to determine initial conditions require
387 several parameters to control ash particle distribution along a vertical line source or some simplified shape
388 of the initial ash cloud, making it difficult in some cases to generate initial conditions that closely resemble
389 a complex reality.

390 The full range of research issues raised by numerical forecasting of volcanic clouds is diverse. We
391 described in this paper the effect of initial conditions chosen from the output of a 3D plume model on
392 numerical forecasts of volcanic ash transport simulation. The wind field, another important factor in
393 volcanic ash transportation simulation is not discussed in the present work. Some other aspects, such as
394 small scale physical processes, even though they play lesser roles, might need to be included in VATDs to
395 improve accuracy for a particular eruption. In addition, eruption conditions are subject to change with time,
396 even during the climactic phase of an eruption. In the future, time-dependent initial conditions for VATDs
397 can be created from 3D plume simulations with time-dependent eruption conditions.

CONFLICT OF INTEREST STATEMENT

398 The authors declare that the research was conducted in the absence of any commercial or financial
399 relationships that could be construed as a potential conflict of interest.

AUTHOR CONTRIBUTIONS

400 The idea of using 3D plume model to start a VATD simulation originated from a conservation between AP
401 and MB. ZC carried out the Plume-SPH simulations, PUFF simulations, results analysis, and prepared the
402 first draft. All authors worked together for further revisions. MB carried out the HYSPLIT simulation. QY
403 post processed the PUFF simulation results, overlapped the simulation results with satellite observation.
404 All authors contributed equally to the manuscript writing. AP and MB got fundings to financially support
405 the work.

FUNDING

406 Details of all funding sources should be provided, including grant numbers if applicable. Please ensure to
407 add all necessary funding information, as after publication this is no longer possible.

ACKNOWLEDGMENTS

408 Support for the Twentieth Century Reanalysis Project dataset is provided by the U.S. Department of Energy,
409 Office of Science Innovative and Novel Computational Impact on Theory and Experiment (DOE INCITE)
410 program, and Office of Biological and Environmental Research (BER), and by the National Oceanic and
411 Atmospheric Administration Climate Program Office.

REFERENCES

- 412 Avdyushin, S., Tulinov, G., Ivanov, M., Kuzmenko, B., Mezhuev, I., Nardi, B., et al. (1993). 1. spatial and
413 temporal evolution of the optical thickness of the pinatubo aerosol cloud in the northern hemisphere
414 from a network of ship-borne and stationary lidars. *Geophysical research letters* 20, 1963–1966
- 415 Bonadonna, C. and Houghton, B. (2005). Total grain-size distribution and volume of tephra-fall deposits.
416 *Bulletin of Volcanology* 67, 441–456
- 417 Bursik, M. (2001). Effect of wind on the rise height of volcanic plumes. *Geophys. Res. Lett* 28, 3621–3624
- 418 Bursik, M., Jones, M., Carn, S., Dean, K., Patra, A., Pavolonis, M., et al. (2012). Estimation and
419 propagation of volcanic source parameter uncertainty in an ash transport and dispersal model: application
420 to the eyjafjallajokull plume of 14–16 april 2010. *Bulletin of volcanology* 74, 2321–2338
- 421 Cao, Z., Patra, A., Bursik, M., Pitman, E. B., and Jones, M. (2018). Plume-sph 1.0: a three-dimensional,
422 dusty-gas volcanic plume model based on smoothed particle hydrodynamics. *Geoscientific Model
Development* 11, 2691–2715
- 423 Cao, Z., Patra, A., and Jones, M. (2017). Data management and volcano plume simulation with parallel
425 sph method and dynamic halo domains. *Procedia Computer Science* 108, 786–795
- 426 Cerminara, M., Esposti Ongaro, T., and Berselli, L. (2016a). Ashee-1.0: a compressible, equilibrium-
427 eulerian model for volcanic ash plumes. *Geoscientific Model Development* 9, 697–730
- 428 Cerminara, M., Esposti Ongaro, T., and Neri, A. (2016b). Large eddy simulation of gas–particle kinematic
429 decoupling and turbulent entrainment in volcanic plumes. *Journal of Volcanology and Geothermal
Research*
- 431 Compo, G. P., Whitaker, J. S., and Sardeshmukh, P. D. (2006). Feasibility of a 100-year reanalysis using
432 only surface pressure data. *Bulletin of the American Meteorological Society* 87, 175–190

- 433 Compo, G. P., Whitaker, J. S., Sardeshmukh, P. D., Matsui, N., Allan, R. J., Yin, X., et al. (2011). The
434 twentieth century reanalysis project. *Quarterly Journal of the Royal Meteorological Society* 137, 1–28
- 435 Costa, A., Suzuki, Y., Cerminara, M., Devenish, B., Esposti Ongaro, T., Herzog, M., et al. (2016). Results
436 of the eruptive column model inter-comparison study. *Journal of Volcanology and Geothermal Research*
- 437 D'amours, R. (1998). Modeling the etex plume dispersion with the canadian emergency response model.
438 *Atmospheric Environment* 32, 4335–4341
- 439 Daniele, P., Lirer, L., Petrosino, P., Spinelli, N., and Peterson, R. (2009). Applications of the puff model to
440 forecasts of volcanic clouds dispersal from etna and vesuvio. *Computers & Geosciences* 35, 1035–1049
- 441 DeFoor, T. E., Robinson, E., and Ryan, S. (1992). Early lidar observations of the june 1991 pinatubo
442 eruption plume at mauna loa observatory, hawaii. *Geophysical research letters* 19, 187–190
- 443 de'Michieli Vitturi, M., Neri, A., and Barsotti, S. (2015). Plume-mom 1.0: A new integral model of
444 volcanic plumes based on the method of moments. *Geoscientific Model Development* 8, 2447–2463
- 445 Deshler, T., Hofmann, D., Johnson, B., and Rozier, W. (1992). Balloonborne measurements of the pinatubo
446 aerosol size distribution and volatility at laramie, wyoming during the summer of 1991. *Geophysical
447 research letters* 19, 199–202
- 448 Draxler, R. R. and Hess, G. (1998). An overview of the hysplit-4 modelling system for trajectories.
449 *Australian meteorological magazine* 47, 295–308
- 450 Fero, J., Carey, S. N., and Merrill, J. T. (2008). Simulation of the 1980 eruption of mount st. helens using
451 the ash-tracking model puff. *Journal of Volcanology and Geothermal Research* 175, 355–366
- 452 Fero, J., Carey, S. N., and Merrill, J. T. (2009). Simulating the dispersal of tephra from the 1991
453 pinatubo eruption: implications for the formation of widespread ash layers. *Journal of Volcanology and
454 Geothermal Research* 186, 120–131
- 455 Folch, A., Costa, A., and Macedonio, G. (2009). Fall3d: A computational model for transport and
456 deposition of volcanic ash. *Computers & Geosciences* 35, 1334–1342
- 457 Folch, A., Costa, A., and Macedonio, G. (2016). Fplume-1.0: An integral volcanic plume model accounting
458 for ash aggregation. *Geoscientific Model Development* 9, 431
- 459 Guo, S., Bluth, G. J., Rose, W. I., Watson, I. M., and Prata, A. (2004a). Re-evaluation of so2 release
460 of the 15 june 1991 pinatubo eruption using ultraviolet and infrared satellite sensors. *Geochemistry,
461 Geophysics, Geosystems* 5
- 462 Guo, S., Rose, W. I., Bluth, G. J., and Watson, I. M. (2004b). Particles in the great pinatubo volcanic cloud
463 of june 1991: The role of ice. *Geochemistry, Geophysics, Geosystems* 5
- 464 Holasek, R., Self, S., and Woods, A. (1996a). Satellite observations and interpretation of the 1991 mount
465 pinatubo eruption plumes. *Journal of Geophysical Research: Solid Earth* 101, 27635–27655
- 466 Holasek, R. E., Woods, A. W., and Self, S. (1996b). Experiments on gas-ash separation processes in
467 volcanic umbrella plumes. *Journal of volcanology and geothermal research* 70, 169–181
- 468 Jäger, H. (1992). The pinatubo eruption cloud observed by lidar at garmisch-partenkirchen. *Geophysical
469 research letters* 19, 191–194
- 470 Mastin, L. G. (2007). A user-friendly one-dimensional model for wet volcanic plumes. *Geochemistry,
471 Geophysics, Geosystems* 8
- 472 Neri, A., Esposti Ongaro, T., Macedonio, G., and Gidaspow, D. (2003). Multiparticle simulation of
473 collapsing volcanic columns and pyroclastic flow. *Journal of Geophysical Research: Solid Earth*
474 (1978–2012) 108
- 475 Oberhuber, J. M., Herzog, M., Graf, H.-F., and Schwanke, K. (1998). Volcanic plume simulation on large
476 scales. *Journal of Volcanology and Geothermal Research* 87, 29–53

- 477 Paladio-Melosantos, M. L. O., Solidum, R. U., Scott, W. E., Quiambao, R. B., Umbal, J. V., Rodolfo, K. S.,
478 et al. (1996). Tephra falls of the 1991 eruptions of mount pinatubo. *Fire and mud* 12000, 12030
- 479 Pouget, S., Bursik, M., Singla, P., and Singh, T. (2016). Sensitivity analysis of a one-dimensional model of
480 a volcanic plume with particle fallout and collapse behavior. *Journal of Volcanology and Geothermal*
481 *Research*
- 482 Rolph, G., Stein, A., and Stunder, B. (2017). Real-time environmental applications and display system:
483 Ready. *Environmental Modelling & Software* 95, 210–228
- 484 Schwaiger, H. F., Denlinger, R. P., and Mastin, L. G. (2012). Ash3d: A finite-volume, conservative
485 numerical model for ash transport and tephra deposition. *Journal of Geophysical Research: Solid Earth*
486 117
- 487 Scott, W. E., Hoblitt, R. P., Torres, R. C., Self, S., Martinez, M. M. L., and Nillos, T. (1996). Pyroclastic
488 flows of the june 15, 1991, climactic eruption of mount pinatubo. *Fire and Mud: eruptions and lahars of*
489 *Mount Pinatubo, Philippines*, 545–570
- 490 Searcy, C., Dean, K., and Stringer, W. (1998). Puff: A volcanic ash tracking and prediction model. *Journal*
491 *of Volcanology and Geothermal Research* 80, 1–16
- 492 Self, S., Zhao, J.-X., Holasek, R. E., Torres, R. C., and King, A. J. (1996). The atmospheric impact of the
493 1991 mount pinatubo eruption
- 494 Stein, A., Draxler, R., Rolph, G., Stunder, B., Cohen, M., and Ngan, F. (2015). Noaa's hysplit atmospheric
495 transport and dispersion modeling system. *Bulletin of the American Meteorological Society* 96, 2059–
496 2077
- 497 Stohl, A., Prata, A., Eckhardt, S., Clarisse, L., Durant, A., Henne, S., et al. (2011). Determination of
498 time-and height-resolved volcanic ash emissions and their use for quantitative ash dispersion modeling:
499 the 2010 eyjafjallajökull eruption. *Atmospheric Chemistry and Physics* 11, 4333–4351
- 500 Suzuki, T. et al. (1983). A theoretical model for dispersion of tephra. *Arc volcanism: physics and tectonics*
501 95, 113
- 502 Suzuki, Y. and Koyaguchi, T. (2009). A three-dimensional numerical simulation of spreading umbrella
503 clouds. *Journal of Geophysical Research: Solid Earth (1978–2012)* 114
- 504 Suzuki, Y. J., Koyaguchi, T., Ogawa, M., and Hachisu, I. (2005). A numerical study of turbulent mixing
505 in eruption clouds using a three-dimensional fluid dynamics model. *Journal of Geophysical Research:*
506 *Solid Earth* 110
- 507 Tanaka, H. (1991). Development of a prediction scheme for the volcanic ash fall from redoubt volcano. In
508 *First Int'l. Symp. on Volcanic Ash and Aviation Safety*. vol. 58
- 509 Tupper, A., Itikarai, I., Richards, M., Prata, F., Carn, S., and Rosenfeld, D. (2007). Facing the challenges of
510 the international airways volcano watch: the 2004/05 eruptions of manam, papua new guinea. *Weather*
511 *and Forecasting* 22, 175–191
- 512 Walko, R., Tremback, C., and Bell, M. (1995). Hypact: The hybrid particle and concentration transport
513 model. *User's guide*
- 514 Whitaker, J. S., Compo, G. P., Wei, X., and Hamill, T. M. (2004). Reanalysis without radiosondes using
515 ensemble data assimilation. *Monthly Weather Review* 132, 1190–1200
- 516 Witham, C., Hort, M., Potts, R., Servranckx, R., Husson, P., and Bonnardot, F. (2007). Comparison of
517 vaac atmospheric dispersion models using the 1 november 2004 grimsvötn eruption. *Meteorological*
518 *Applications* 14, 27–38
- 519 Woods, A. (1988). The fluid dynamics and thermodynamics of eruption columns. *Bulletin of Volcanology*
520 50, 169–193

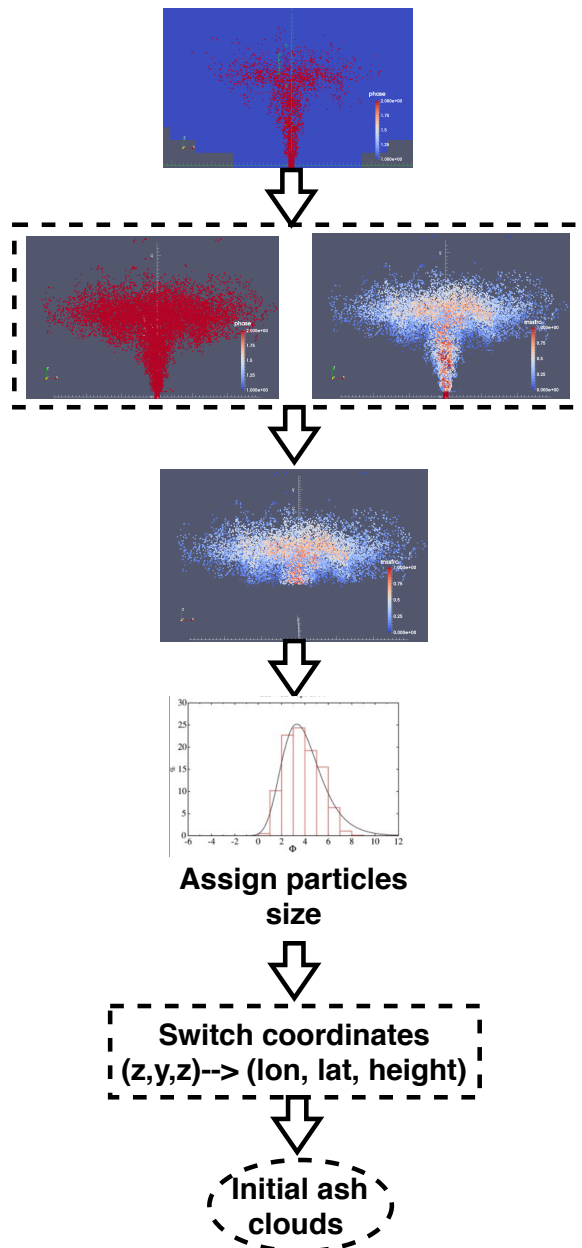


Figure 1. Workflow to create initial condition for Puff based on raw output of Plume-SPH (Cao et al., 2018). Top: raw output of Plume-SPH. Blue particles are phase 1 (ambient air), red particles are phase 2 (erupted material). Second row: plume after removing SPH particles of phase 1. Left: colored according to mass fraction of erupted material. Third row: volcanic plume above the “corner” region after cutting off the lower portion. Forth row: assign sizes to particles converting numerical discretization points into tracers. Fifth row: switch coordinates in local coordinate system into (*longitude, latitude, height*)

521 Zidikheri, M. J., Lucas, C., and Potts, R. J. (2017). Estimation of optimal dispersion model source
 522 parameters using satellite detections of volcanic ash. *Journal of Geophysical Research: Atmospheres*
 523 122, 8207–8232

FIGURE CAPTIONS

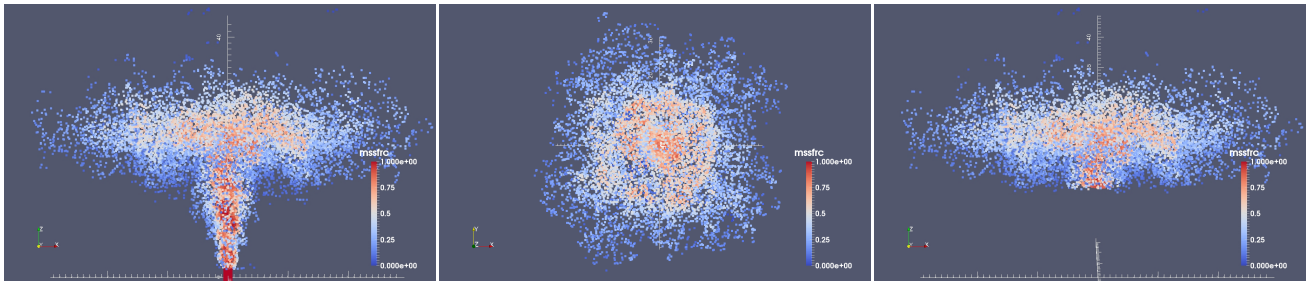


Figure 2. Volcano plume from 3D plume model. All particles in the pictures are of type phase 2 (phase 1 has been removed in step 1) at 600s after eruption, at which time, the plume has already reached the maximum height and started spreading radially. Pictures from left to right are: front view of the whole plume, top view of the plume and front view of the initial ash cloud, which is essentially a portion of the whole plume with elevation higher than a given threshold (in this picture is 15000m). Particles are colored according to mass fraction of erupted material. Red represents high mass fraction while blue represents low mass fraction.

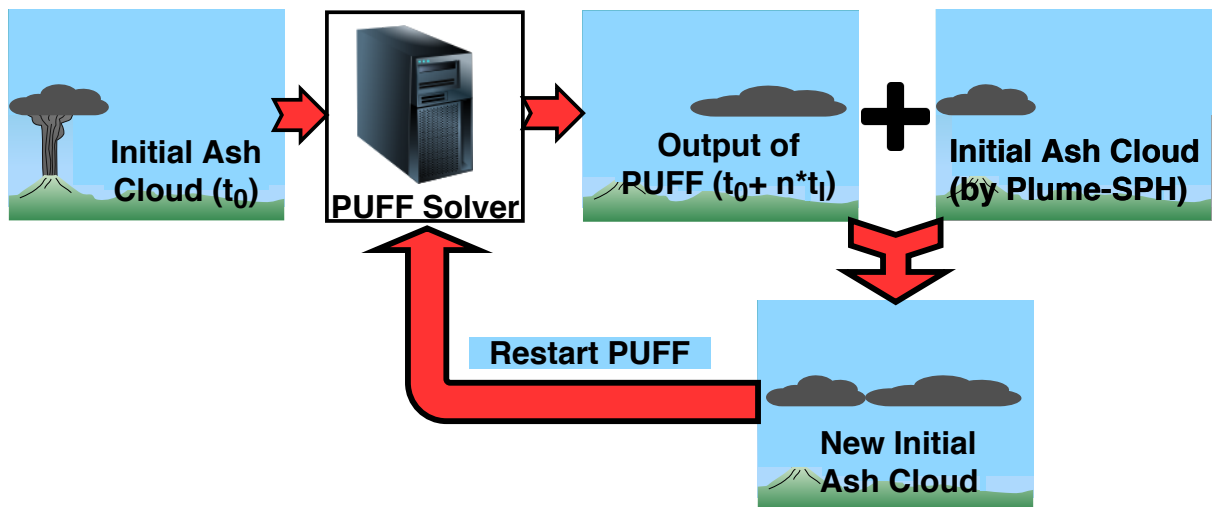


Figure 3. Mimic successive eruption with intermittent pulsed releasing of ash particles. t_I is the period of pulsing release. t_I equals the physical time of 3D plume simulation.

Table 1. Three different methods for creating initial conditions (initial ash clouds) for Puff simulation

	No model	1D model	3D model
Maximum height	Calibration	Semiempirical	1st principle
Average height	Calibration	Conservation laws (1D)	1st principle
Vertical spread	Calibration	Semiempirical	1st principle
Column radius	Calibration	Conservation laws (1D)	1st principle
Plume shape	Semiempirical	Semiempirical	1st principle
Tracers number	Free parameter	Free Parameter	Based on simulation

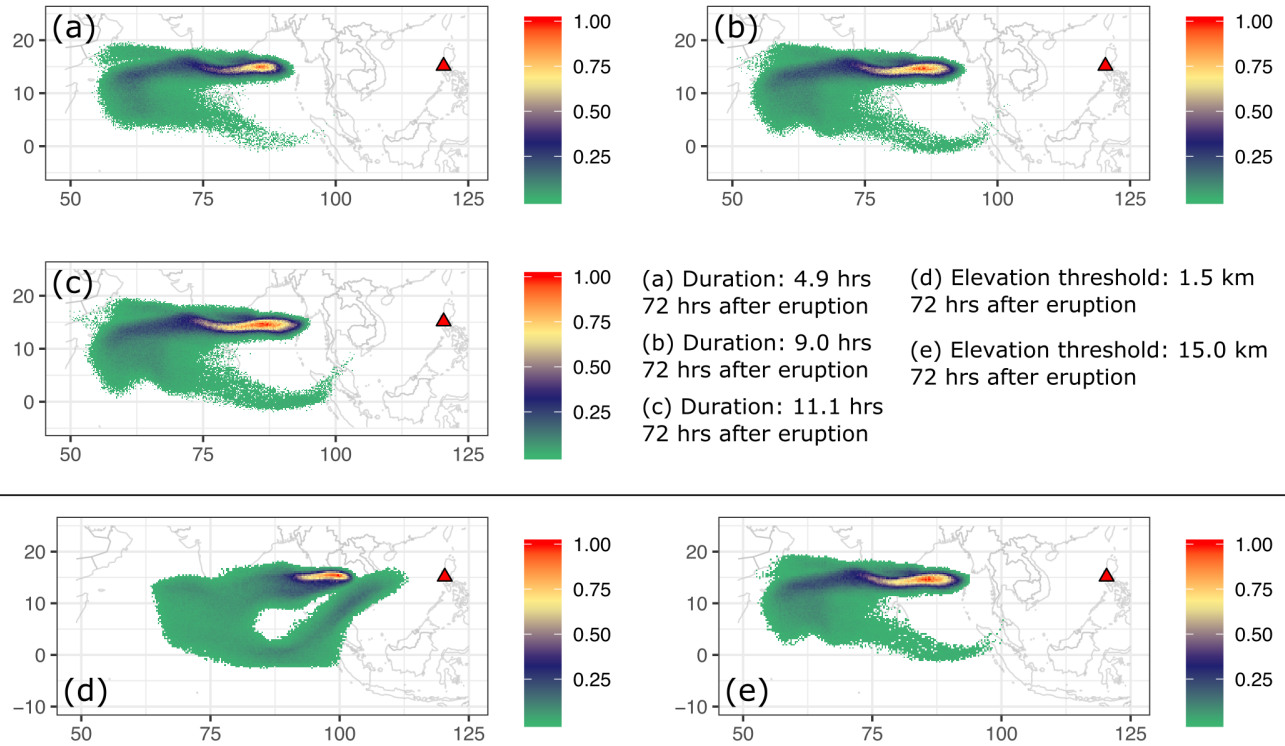


Figure 4. Sensitivity of Puff simulation with respect to eruption durations and initial ash cloud cutoff heights. a) to c) are simulated ash distribution with different starting and ending time. They corresponding to eruption duration of 4.9 hours, 9 hours and 11.1 hours respectively. Starting and ending time for each case is in Table 2. d) and e) are simulated ash distribution taking initial ash clouds obtained using different elevation thresholds (1500m and 15000 m) from output of Plume-SPH. The starting and ending time are corresponding to 9 hours duration case in Table 2. The contours correspond to ash concentration at 72 hours after eruption.

Table 2. The starting and ending time (UT) for simulating the climactic phase of Pinatubo eruption on June 15 1991. Observed plume height (Holasek et al., 1996a) at different time are also listed in the table.

Eruption duration	4.9 hours	9 hours	10 hours	11.1 hours
Start time	0441	0441	0441	0334
Height at start time	37.5 km	37.5 km	37.5 km	24.5 km
End time	0934	1341	1441	1441
Height at end time	35 km	26.5 km	22.5	22.5 km

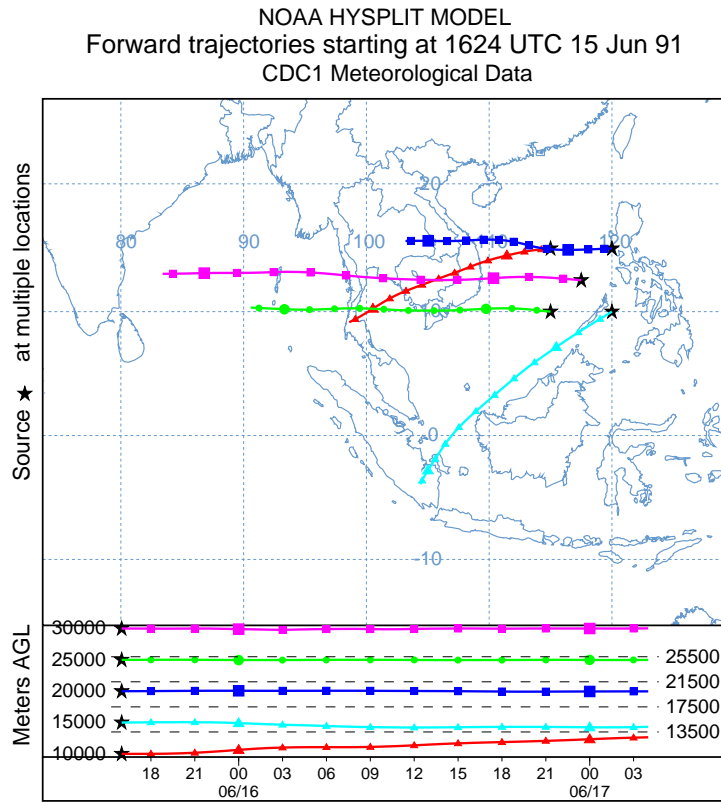


Figure 5. Trajectories of particles starting from different heights indicating the wind directions of different evaluations.

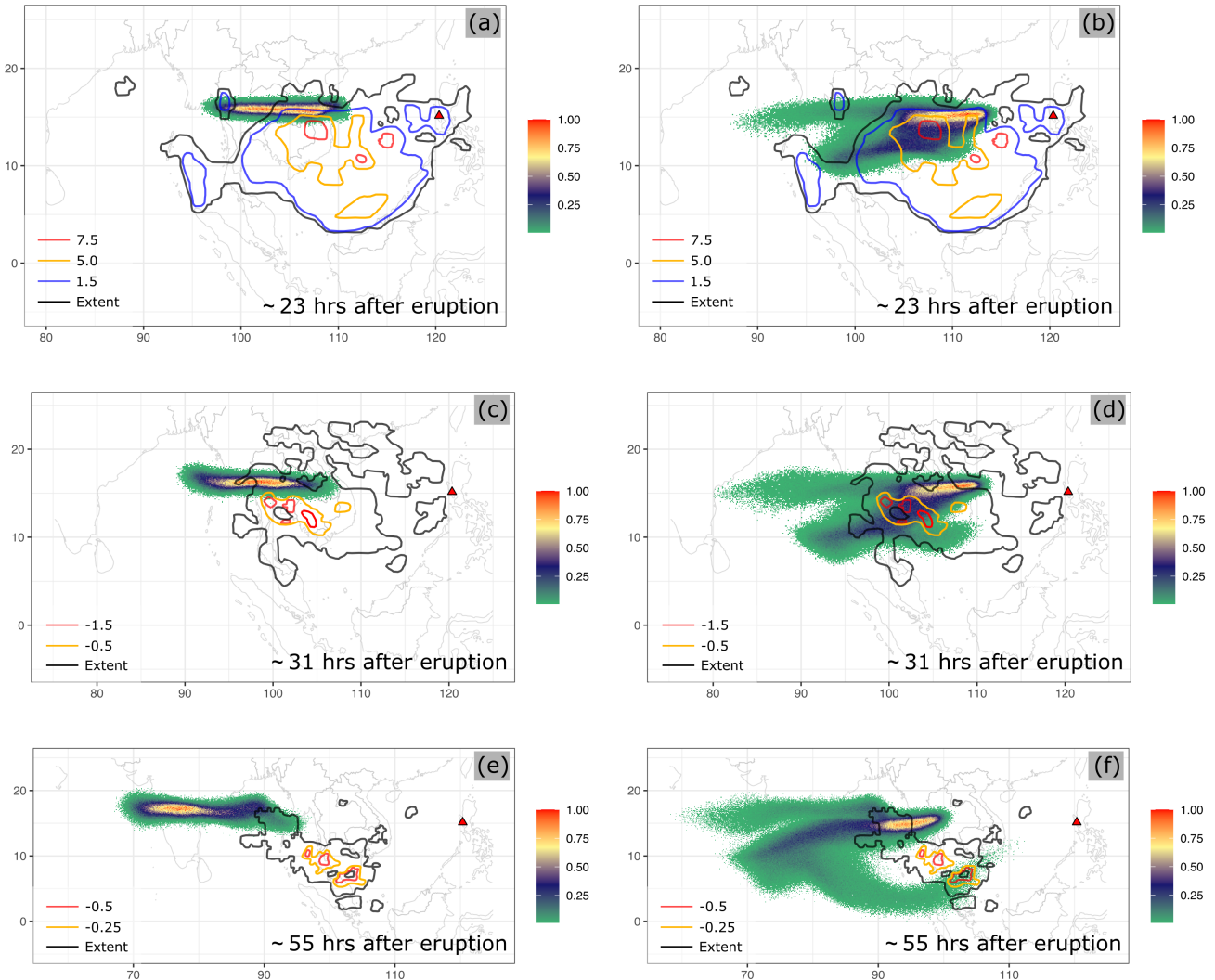


Figure 6. Comparison between “Semiempirical initial cloud + Puff” and “Plume-SPH + Puff”. Pictures to the left are: Puff simulation based on initial condition created according to semiempirical plume shape expression. Pictures to the right are Puff simulation based on initial condition generated by Plume-SPH. TOMS or AVHRR image of Pinatubo ash cloud are overlapped with the simulation results. Ash clouds at different hours after eruption are on different rows. From top to bottom, the images are corresponding to around 23 hours after eruption (UT 199106160341), 31 hours after eruption (UT 199106161141), 55 hours after eruption (UT 199106171141). The observation data on the first row are TOMS ash and ice map. The observation data on the second and third row are AVHRR BTD ash cloud map with atmospheric correction method applied (Guo et al., 2004b).

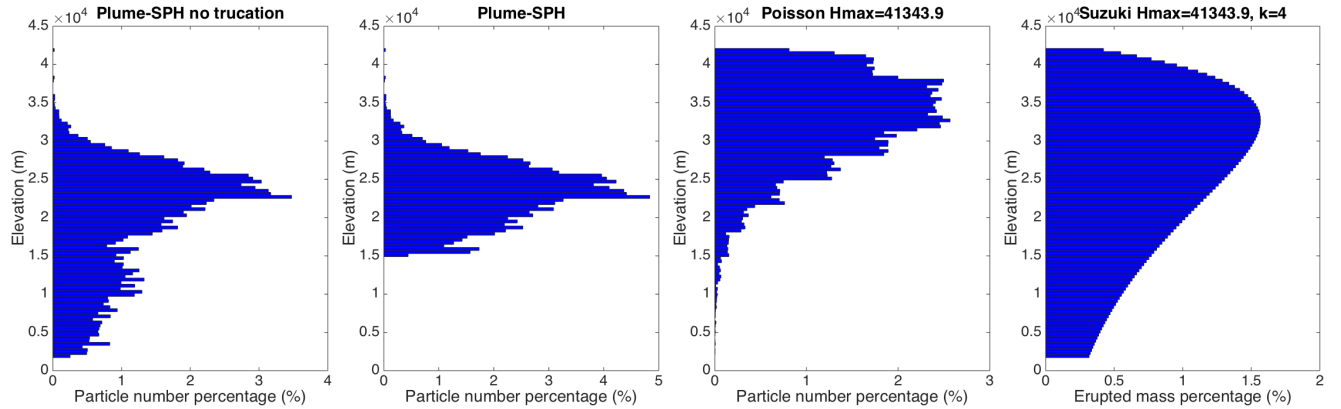


Figure 7. Particle distribution of initial ash cloud in vertical direction. The picture to the left is corresponding to the initial ash cloud obtained from Plume-SPH output. The second picture is corresponding to ash distribution truncated by a elevation threshold of 15000m. The third picture is for vertical ash distribution based on Poisson distribution with maximum height equals to 40000m. Another parameter, the vertical spread, in the expression of Poisson plume shape is 6662m. The picture to the right is corresponding to Suzuki distribution with maximum height equals to 40000m. Another parameter in Suzuki distribution, the shape factor, is 4. The x axis is the percentage of particle numbers for Plume-SPH and Poisson. For Suzuki the x axis is the mass percentage of erupted material.

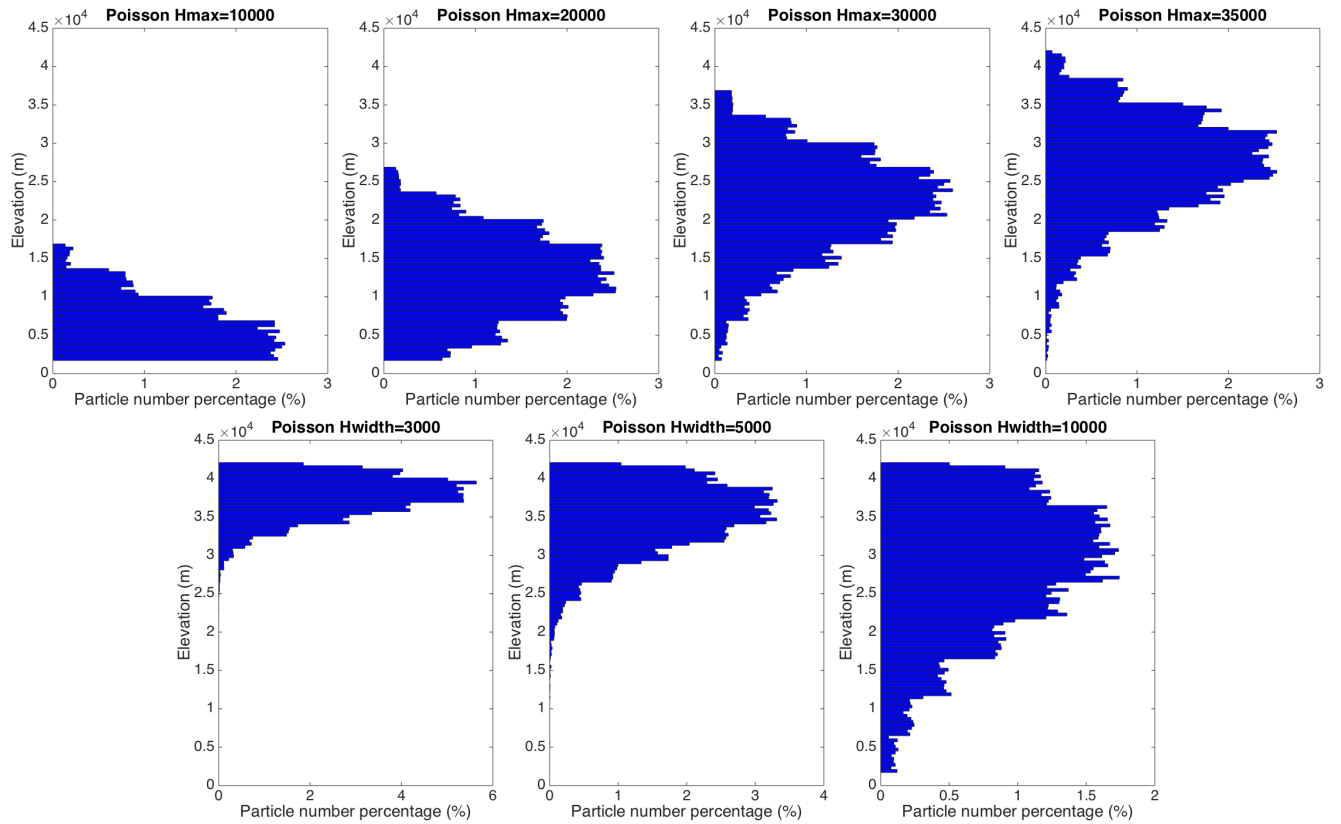


Figure 8. Initial particle distribution in vertical direction based on Poisson plume shape. The first row varies maximum heights. Pictures from left to right are corresponding to maximum height of 10000m, 20000m, 30000m, 35000m. Another parameter, the vertical spread, in the expression of Poisson plume shape is 6662m for all four figures. The second row varies “vertical spread”. Pictures from left to right are corresponding to vertical spread of 3km, 5km and 10km. The maximum height in the expression of Poisson plume shape is 40000m for all three figures. The x axis is the percentage of particle numbers. See Fig. 7 for vertical ash distribution of Plume-SPH output.

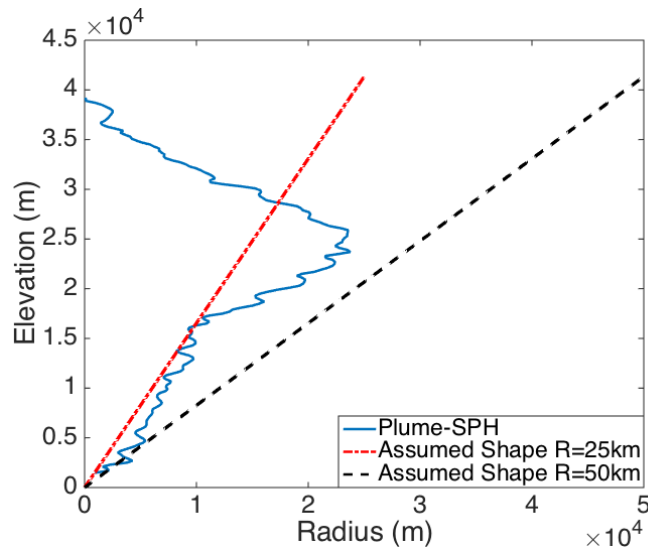


Figure 9. Comparison between radius of initial ash clouds created by 3D plume model (Plume-SPH) and assumed initial ash cloud shape in Puff. The plume shape expression used in Puff defines an inverted cone whose actual shape changes when “horizontal spread” takes different values. $R = 25\text{km}$ is corresponding to “horizontal spread” equals to 50km . $R = 50\text{km}$ is corresponding to “horizontal spread” equals to 100km

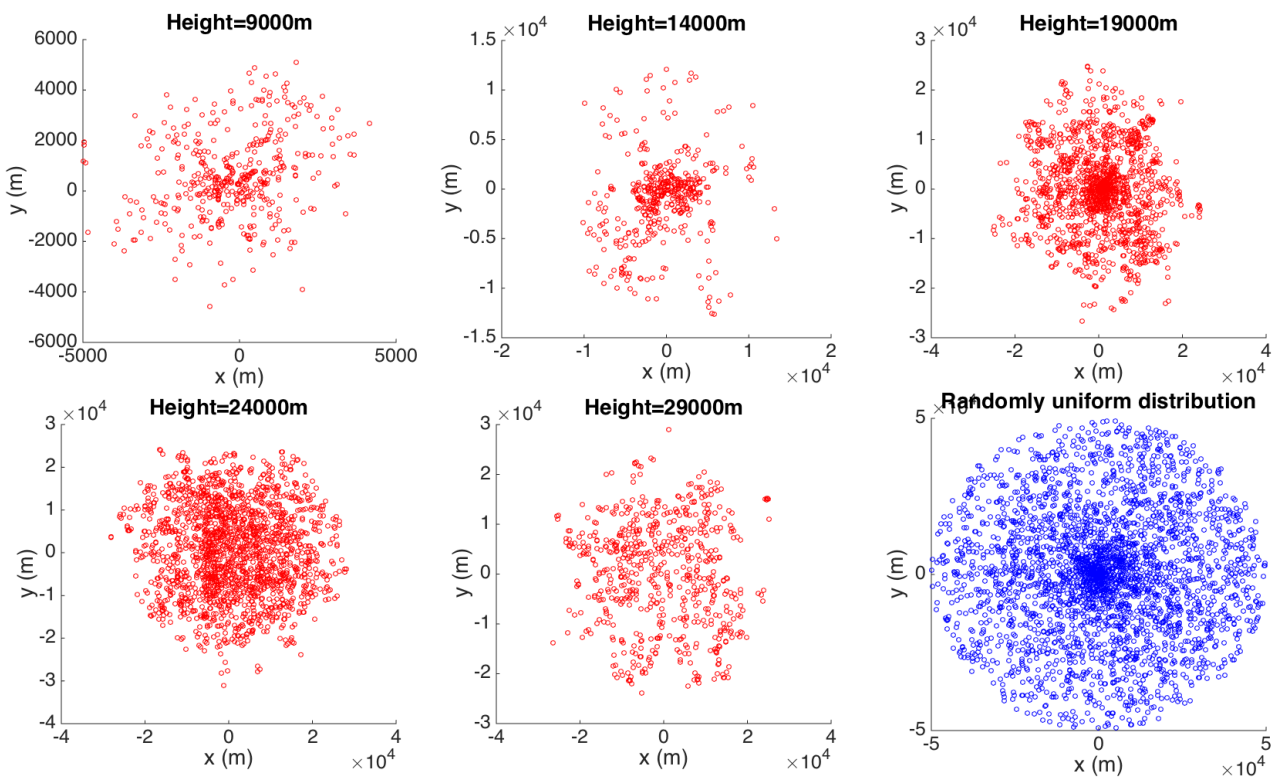


Figure 10. Horizontal distribution of ash particles (tracers) on a cross section of initial ash cloud. Puff assumes a randomly uniform distribution of ash particles within a circle, as shown by blue dots in the last figure. All other figures show the ash particle distribution of initial ash clouds created by Plume-SPH at different elevations.

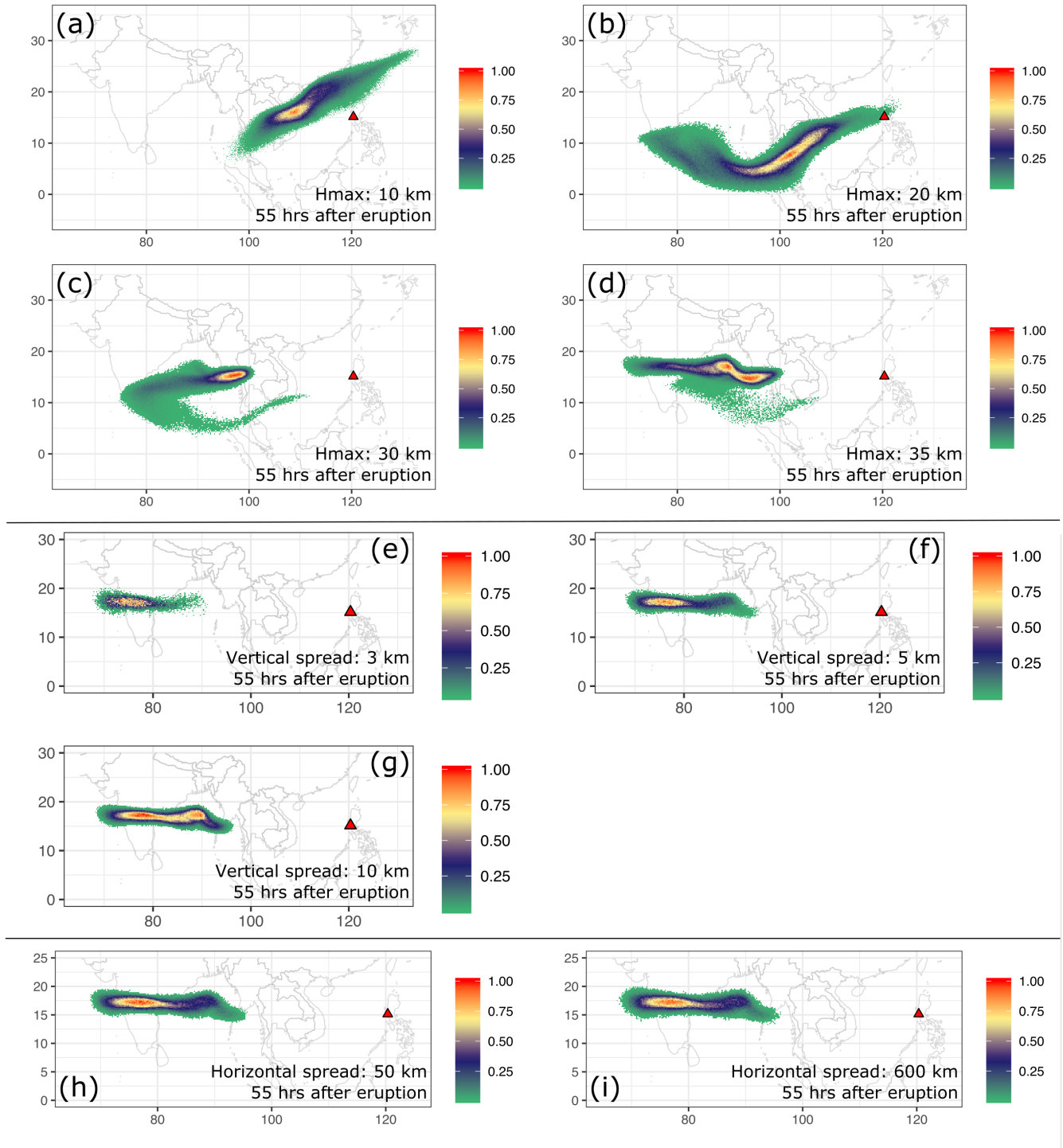


Figure 11. Ash transportation simulated by Puff using different initial ash clouds created according the empirical expressions. Initial ash cloud for a) to d) are created according to Poisson distribution with maximum plume heights of 10km, 20km, 30km and 35km respectively. Initial ash cloud for e) to g) are created with vertical spread equals to 3km, 5km and 10km. respectively. Initial ash cloud for h) - i) are created with “horizontal spread” equals to 50km and 600km respectively. All images are for simulated ash transportation around 55 hours after eruption (UT 199106171141). See the observed cloud image in Fig. 6.

Table 3. List of eruption condition and material properties for plume simulation

Parameters	Units	Plume
Vent velocity	$m \cdot s^{-1}$	275
Vent gas mass fraction		0.05
Vent Temperature	K	1053
Vent height	m	1500
Mass discharge rate	$kg \cdot s^{-1}$	1.5×10^9
Specific heat of gas at constant volume	$J \cdot kg^{-1} \cdot K^{-1}$	717
Specific heat of air at constant volume	$J \cdot kg^{-1} \cdot K^{-1}$	1340
Specific heat of solid	$J \cdot kg^{-1} \cdot K^{-1}$	1100
Specific heat of gas at constant pressure	$J \cdot kg^{-1} \cdot K^{-1}$	1000
Specific heat of air at constant pressure	$J \cdot kg^{-1} \cdot K^{-1}$	1810
Density of air at vent height	$kg \cdot m^{-3}$	1.104
Pressure at vent height	Pa	84363.4

Table 4. Parameters used in VATD simulation of the climactic phase of Pinatubo eruption on June 15 1991. The first six parameters are used by semiempirical expression to create an initial ash cloud. When creating an initial condition based on the Plume-SPH model, these parameters are extracted from output of Plume-SPH model.

Parameters	Unit	Semiempirical	Plume-SPH
Maximum Height (H_{max})	m	40000	41800
Horizontal Spread (R_{max})	km	103.808	-
Vertical Spread (H_{width})	km	6.662	-
Plume Shape	-	Poisson	-
Total Ash Particles	-	1768500	1768500
Elevation Threshold	m	-	15000
Horizontal Diffusivity	m^2/s	10000	10000
Vertical Diffusivity	m^2/s	10	10
Grain Size Distribution	-	Gaussian	Gaussian
Mean of Grain Size (Radius)	mm	3.5×10^{-2}	3.5×10^{-2}
Standard Deviation of Grain Size	-	1.0	1.0
Start Time	UT	0441	0441
End time	UT	1341	1341
Simulation Duration	hour	72	72